This document is downloaded from DR-NTU (https://dr.ntu.edu.sg)
Nanyang Technological University, Singapore.

Effects of axial compression load and eccentricity on seismic behaviour of nonseismically detailed interior beam-wide column joints

Li, Bing; Pan, Tso-Chien; Tran, Cao Thanh Ngoc

2009

Li, B., Pan, T. C., & Tran, C. T. N. (2009). Effects of axial compression load and eccentricity on seismic behaviour of nonseismically detailed interior beam-wide column joints. Journal of Structural Engineering, 135(7), 774–784.

https://hdl.handle.net/10356/95771

https://doi.org/10.1061/(ASCE)0733-9445(2009)135:7(774)

© 2009 ASCE. This is the author created version of a work that has been peer reviewed and accepted for publication by Journal of structural engineering, ASCE. It incorporates referee’ s comments but changes resulting from the publishing process, such as copyediting, structural formatting, may not be reflected in this document. The published version is available at: http://dx.doi.org/10.1061/(ASCE)0733-9445(2009)135:7(774).

Downloaded on 05 Apr 2024 19:50:51 SGT

Effects of Axial Compression Load and Eccentricity on Seismic Behavior of Nonseismically Detailed Interior Beam-Wide Column Joints

Bing Li[1]; Tso-Chien Pan[2]; and Cao Thanh Ngoc Tran[3]

[1]Associate Professor, School of Civil and Environmental Engineering, Nanyang Technological Univ., Singapore 639798, Singapore (corresponding author). E-mail: cbli@ntu.edu.sg

[2]Professor, School of Civil and Environmental Engineering, Nanyang Technological Univ., Singapore 639798, Singapore.

[3]Ph.D. Candidate, School of Civil and Environmental Engineering, Nanyang Technological Univ., Singapore 639798, Singapore.

Abstract: Six full-scale nonseismically detailed reinforced concrete interior beam-wide column joints were tested to investigate the seismic behavior of the joints. Axial compression loads varying from zero to high magnitude, as well as quasi-static cyclic loading simulating earthquake actions were applied. The overall performance of each test assembly was examined in terms of lateral load capacity, drift, stiffness, energy dissipation capacity, and joint shear strength. Three levels of axial compressive column load were investigated to determine how this variable might influence the performance of the joint. The tests also explored the effects of centerline

eccentricity on the performance of interior beam-wide column joints subjected to earthquake loading. All the specimens failed at the joint panel with gradual strength deterioration, low attainment of structural stiffness, and bond degradation. The low attainment of stiffness and strength was attributed to the bond deterioration of the longitudinal bars through the joint core. It is concluded that special reinforced concrete interior beam-wide column joints with nonseismic design and detailing, could possess the inherent ductility for an adequate response to unexpected moderate earthquakes.

CE Database subject headings: Beam columns; Bonding; Reinforced concrete; Axial compression; Seismic effects; Joints.

Introduction

Reinforced concrete structures consisting of wall-like wide column elements are very common in regions of low to moderate seismicity; such structures predominate Singapore structural system. Recent post-earthquake investigations have indicated that the extensive damage to the beam-wide column joints in nonseismically detailed frames is the result of excessive shear deformation and severe strength degradation. These can eventually lead to a structural collapse. The BS 8110 (BSI 1997) code used in Singapore does not specify any provisions for seismic design or detailing of reinforced concrete structures. Therefore, it is of great concern that the strength, ductility, and energy dissipation capacity of these structures may not be adequate to sustain earthquake-induced loads in regions of low to moderate seismicity. The needs for evaluating and improving the detailing of such existing structures are obvious.

In an eccentric joint, the column centerline is offset from the beam centerline. When an eccentric beam-column joint is subjected to seismic loadings, the eccentricity between beam

and column centerlines induces torsional moment in the joint region as illustrated in Fig. 1. This produces additional joint shear stresses. Extensive experimental research on concentric interior beam-column joints, conducted in different countries in the past decade, has given a better understanding of the behavior of the concentric joints. Unlike the large database of concentric joints, only limited amounts of experimental test results are available for eccentric joints. The following are the experimental works on eccentric interior beam-column joints.

Joh et al. (1991) reported a series of five tests on large-scale interior beam-column joints, including two eccentric joints. It was found that the displacement ductility of the eccentric joints was much smaller than the concentric joints. The joint shear deformation at the flush side of the joint was four to five times larger than those at the offset side of the joint.

Lawrance et al. (1991) carried out tests on two interior beam-column joints, which included one eccentric joint. The eccentricity was found to have no effect on the global strength of the specimen. The strength degradation in the eccentric specimen was observed to occur at a lower displacement ductility than in the companion concentric specimen.

Raffaelle and Wight (1995) reported the test results of four reinforced concrete eccentric interior beam-column joints. The major design parameters that varied in the specimens were the beam width, the beam depth, and the amount of top and bottom longitudinal reinforcement in the beam. Based on the test results, it was concluded that the presence of eccentricity in the joint reduced the joint strength to an extent that none of the specimens were able to attain their predicted story shear strength.

Teng and Zhou (2003) conducted tests on six large-scale interior beam-column joints designed according to ACI-ASCE 352 recommendations (ACI-ASCE 1985). The variables in the specimens were the joint eccentricity and the cross section of column. All specimens were

subjected to a column axial load level of $0.08f'_cA_g$. Teng and Zhou (2003) found that ACI 318 formula (ACI 2002) for the effective joint width was conservative, while NZS 3101 (Standards New Zealand 1995) and AIJ (1994) formulas might not be conservative. Even though joint eccentricity slightly reduced the story strength, the influence on the energy-dissipating capacity and average joint shear deformation of the specimens was not always observed.

Shin and LaFave (2004) carried out tests on two 2/3-scale reinforced concrete eccentric beam-column-slab subassemblies, which were designed according to ACI 318-02 (ACI 2002). The main design variables in the specimens were the centerline eccentricity between beam and column and the edge-beam width. Shin and LaFave (2004) found that both specimens exhibited similar behavior even though one of them had larger eccentricity and narrower beam configuration. Both reached the same joint shear strength before they started to break down. It was concluded that floor slabs diminished the differences between seismic performances of these eccentric joints and increased joint shear strengths of the specimens. The current ACI code procedures (ACI 2002) for estimating nominal joint shear strength were quite conservative for the case of the tested eccentric beam-column joints with floor slabs. Shin and LaFave (2004) recommended an effective joint width equal to the average of beam and column widths be used to estimate the joint shear strength of eccentric beam-column joint.

Reviewing the previous studies (Joh et al.1991; Lawrance et al. 1991; Raffaelle and Wight 1995; Teng and Zhou 2003; Shin and LaFave 2004) in the area of eccentric interior beam-column joints, the following problem was identified. The effects of axial compressive column load had not been studied in previous research. An experiment has therefore been undertaken at NTU, Singapore, to better understand the effects of axial compressive column load on the seismic behavior of nonseismically detailed eccentric interior beam-wide column joints. The

investigation results will be useful in identifying the seismic weaknesses of such types of beam-column joints. With better knowledge of the deficiencies, it is possible to improve the survivability of reinforced concrete beam-wide column joints during earthquakes.

This paper reports the experimental results of six full-scale special reinforced concrete interior beam-wide column joints often found in framed structures with nonseismic detailing in Singapore. The variables in the test specimens were the level of axial compressive load in the columns and the centerline eccentricity between beam and column. The research reported here is concerned with seismic performance of nonseismically detailed reinforced concrete beam-wide column joints. The study investigates whether the joints are adequate to resist earthquakes.

Experimental Studies

Specimens and Test Setup

Based on BS 8110 code (BSI 1997), six full-scale nonseismically detailed interior beam-wide column joints were constructed and tested. These specimens were typical as-built joints abstracted from the existing buildings in Singapore. Figs. 2 and 3 illustrate the schematic dimensions of specimens. Specimens E1A, E1B, and E1C are eccentric interior beam-column joints with the beam flushed with the column edge, whereas Specimens C1A, C1B, and C1C are concentric interior beam-column joints with their respective centerlines of beams and columns intersecting. These interior beam-wide column joints have a column to beam width ratio of about 3.56, a column cross-section dimension of 820 X 280 mm, and a beam cross-section dimension of 230 X 300 mm. As shown in Table 1, the ratios of column moments over beam moments are very high for all specimens.

The test setup is shown in Fig. 4. Each specimen was subjected to quasi-static reversal

cyclic loads simulating earthquake loadings. A reversible horizontal load was applied to the top of the columns using a double-acting 1,000 kN capacity long-stroke dynamic actuator mounted on the reaction wall. The actuator was pinned at the end to allow rotation during the test. This loading device was manually operated in order to have a better control on the load increment. The bottom of the column was pinned to a strong floor. As for the beam-ends, they were connected to the strong floor by steel links that allowed rotation as well as free horizontal beam movement. Vertical movement of the beam ends was restricted to provide the vertical steel beams with support reactions. The axial compression load was applied using three small hydraulic jacks placed between the column top end and bottom suffix of the steel transfer beam. Four threaded rods were fixed at four corners around the test unit to balance the applied column axial load.

Materials

The specimens were built with identical reinforcement and cast with concrete grade G20. High deformed bars Y10, Y13, Y22, and Y25 were used as main bars in the test units, whereas mild steel bar R10 was used as stirrups.

Test Procedure and Instrumentation

Prior the commencement of each test, the column axial load was progressively applied to the column until the designated level ($0.1f_c'A_g$ for Specimens E1B and C1B or $0.35f_c'A_g$ for Specimens E1C and C1C and zero axial load for Specimens E1A and C1A) was achieved. During each test, the column axial load was maintained by manually adjusting the flat jacks after each loading step. The lateral load was applied cyclically through the dynamic actuator in

a quasi-static fashion at the top end of the column as shown in Fig. 4. The loading procedure consisting of displacement-controlled steps is illustrated in Fig. 5.

In order to obtain the test results, instrumentations such as dynamic actuator, strain gauges, LVDTs, and displacement transducers were installed in the test setup. The specimens were loaded horizontally using a dynamic actuator while the load applied was recorded in the actuator data acquisition system. The behavior of the reinforcement bars was observed by the strain gauges installed in the bars prior to casting. LVDTs and displacement transducers were installed to observe the behavior of joint core area, beam, and column. The horizontal displacement and torsional deformation were measured by three LVDTs installed at the top column end pin.

Description of Test Behavior

The general behaviors of the test specimens were identified based on the load-displacement hysteresis responses, the visible crack patterns, and the local strains observed in the reinforcements.

Fig. 6 shows the horizontal story shear force versus horizontal displacement hysteresis loops of all specimens. The crack patterns observed during the test are shown in Figs. 7–12. Figs. 13 and 14 exhibit the tensile strain profiles at the peak displacements of each drift ratio for the beam top longitudinal bars and the column longitudinal bars, respectively. The initial stiffness and stiffness degradation trend of all specimens are shown in Fig. 15. Figs. 16 and 17 illustrate the energy dissipation capacity and the displacement decomposition of interstory drift of the specimens, respectively.

Specimen E1A

Specimen E1A was an eccentric interior beam-column with a zero axial load. The measured horizontal story shear force versus horizontal displacement hysteresis loops and the successive crack patterns are shown in Figs. 6(a) and 7, respectively. The maximum load in the positive cycles of loading was 29.7 kN, attained in the first cycle of a drift ratio of 3.0%, whereas in the negative loading cycle, the maximum horizontal load strength measured was 28.9 kN. Both of them were greater than the ideal load strength at the corresponding story drift ratio. Although stirrups were absent in the joint core, the structure still managed to resist horizontal loading up to drift ratio of 4.0% without any significant reduction of load-carrying capacity. As shown in Fig. 16, the specimen had shown good energy dissipation characteristics as the drift ratio increased progressively throughout the test. Maximum energy dissipation of 11.8 kN m was observed at a drift ratio of 4.0%. Fig. 7 illustrates the formation of cracking patterns of E1A. Diagonal flexural cracks were found at both the top and bottom of the E1A beam during a drift ratio of 0.4%. The cracks propagated rapidly with the drift ratio increasing to 1.0%. When drift ratio of 1.0% was attained, a joint core crack was observed at the flushed surface of the beam-column joint. As shown in Fig. 7, when the drift ratio was increased to 3.0 and 4.0%, torsional cracks at both sides of the column were observed. The cracks on the protruded joint at the opposite face were observed at a drift ratio of 3.0%. These cracks were believed to be the extension of the torsional cracks formed at side faces of the column. Fig. 17(a) shows the components of the horizontal displacement measured for E1A at the peak of the selected loading cycles. They are expressed as a percentage of the story drift angle. According to Fig. 17(a), the contribution of beam flexure, beam shear, column flexure, and joint to the total drift were 62.0, 0.7, 12.7, and 12.4%, respectively. The contribution of beam flexure to the total drift was predominant. The first yield in beam longitudinal reinforcement of E1A was observed at a drift ratio of 2.0%. Yielding was

observed to penetrate to the joint core area at a drift ratio of 3.0%. It was observed that the strains along the column steel bars of E1A were very small; this was supported by little flexural cracks observed at the column during the test. When the beam reached its flexural strength the column was still in the elastic range, indicating a "strong column-weak beam" response. As such, the ratios of column flexural strength to beam flexural strength were large.

Specimen E1B

Eccentric Specimen E1B was an interior beam-column with a column axial load of $0.1f'_cA_g$. The maximum load in the positive cycles of 19.8 kN, which was attained at the first cycle of a drift ratio of 1.33%. In the negative loading cycle, the maximum horizontal load measured was 17.3 kN, also obtained in the first cycle of a drift ratio of 1.33%. In general, the beam-column joint showed steady energy dissipation capacity, as shown in Fig. 6(b), with the energy capacity increased throughout the test. Despite the absence of stirrups in the joint core, the energy dissipation capacity of the specimen was satisfactory. The maximum energy dissipated, 5.56 kN m at a drift ratio of 2.0%, was larger than that of E1A. Fig. 8 illustrates the formation of cracking patterns of E1B. Cracks were first observed at a beam top when drift ratio of 0.4% was exceeded. It was noticeable in Fig. 8 that cracks at beams propagated rapidly when drift ratio was increased to 0.67%. When a drift ratio of 1.0% was attained, cracks were found to propagate rapidly at the beam top as well as the joint core. Even though no crack was found in the column, more cracks were formed at a distance further from the joint core area and new cracks were found at the beam bottom after drift ratio of 1.33%. Due to its drastic drop in lateral resisting capacity during the repeating cycles, the specimen failed at a drift ratio of 2.0%. No spalling of concrete was observed throughout the test. The column was also found to be intact with no cracks when the

test was terminated. It is noteworthy that the joint core cracks were only observed at the flushed surface of the beam-column joint while the protruded joint on the opposite face was intact. Fig. 17(b) shows the components of the horizontal displacement measured for E1B at the peak of the selected loading cycles, expressed as a percentage of the story drift angle. The major source of the story drift was the beam displacement, indicating a "strong column weak beam" response. According to Fig. 17(b), the contribution of beam flexure, beam shear, column flexure, and joint to the total drift at a drift ratio of 2.0% were 75.2, 11.7, 1, and 21.6%, respectively. The contribution of the displacement due to joint shear distortion was between 16.3 and 21.5%. The first yielding in beam longitudinal reinforcement of E1A was observed at a drift ratio of 2.0%. The largest tensile strain of the specimens was detected at the beam-column interface. Similar to E1A, it was observed that the strains along the column steel bars of E1B were very small, indicating a "strong column-weak beam" response.

Specimen E1C

Eccentric Specimen E1C was an interior beam-column with a column axial load of $0.35f'_cA_g$. The maximum load in both positive and negative cycles of loading was around 15.2 kN, which was attained at the first cycle of a drift ratio of 2.0%. The specimen began to deteriorate after a drift ratio of 3.0%. E1C was declared a failure and the test was halted when a drift ratio of 4.0% was attained. E1C showed lower energy dissipation capacity as compared to E1B. The maximum energy dissipated at drift ratio of 2.0% was 3.5 kN m, which is much lower than that of E1B as shown in Fig. 16. Fig. 9 illustrates the formation of cracking patterns of E1C. Initial cracks formed at top portion of the beam during drift ratio of 0.4% and cracks propagated rapidly when drift ratio of 1.0% was attained as illustrated in Fig. 9. It is noteworthy that a crack in the joint core area was first found at a drift ratio of 1.0%. As the drift ratio increased, more cracks were

found to propagate rapidly at the beam top as well as joint core. Generally, no cracks were found on the column and no spalling of concrete was observed. More cracks formed further away from the joint core area, while limited new cracks were found at the beam bottom after a drift ratio of 2.0%. E1C failed at a drift ratio of 3.0% with final crack patterns shown in Fig. 9. Similar to Specimen E1B, the joint core cracks were only observed at the flushed surface of the beam-column joint while no cracks were found on the protruded joint at the opposite face. Fig. 17(c) shows the displacement decomposition of E1C. According to Fig. 17(c), the contribution of beam flexure, beam shear, column flexure, and joint to the total drift, at 2% drift ratio were 72.2, 0.5, 3.4, and 6.5%, respectively. The contribution of beam flexure to the total drift was predominant, varying from 57.7 to 95.6%. The contribution of the displacement due to joint shear distortion was between 2.5 and 7.6%, lower than that of E1A or E1B.

Specimen C1A

Specimen C1A was a concentric interior beam-column with a zero axial load. The measured horizontal story shear force versus horizontal displacement hysteresis loops and the successive crack patterns are shown in Figs. 6(d) and 10, respectively. The maximum load in both positive and negative cycles of loading was around 28.3 kN, which was attained at the first cycle of a drift ratio of 3.0%. It was greater than the ideal load strength at the corresponding story drift ratio. Although stirrups were absent in the joint core area, the structure still managed to resist horizontal load up to a drift ratio of 4.0% without any significant reduction of horizontal load. The maximum energy dissipated was 10.6 kN m at a drift ratio of 4.0%. Fig. 10 illustrates the formation of cracking patterns of C1A. Diagonal flexural cracks were found at the beam bottom and top of C1C during a drift ratio of 0.4%. The cracks propagated rapidly when the drift ratio

was increased to 1.0%. When the drift ratio was increased to 3.0 and 4.0%, respectively, flexural cracks at both sides of the column were observed. The cracks on the protruded joint at the opposite face were observed at a drift ratio of 4.0%. These cracks were believed to be the extension of the flexural cracks formed at the side faces of the column. Fig. 17(d) shows the components of the horizontal displacement measured for C1A According to Fig. 17(d), the contribution of beam flexure, beam shear, column flexure, and joint to the total drift, at 4% drift ratio, were 65.9, 2.2, 13.3, and 1.1%, respectively. The contribution to the total drift of beam flexure was predominant. Due to the three-dimensional nature of the specimen, the transducers placed diagonally in the joint panel could not capture the joint shear deformation. It explained low joint deformations were obtained by C1A.

Specimen C1B

Concentric Specimen C1B was an interior beam-column with a column axial load of $0.1f'_cA_g$. The measured horizontal story shear force versus horizontal displacement hysteresis loops and the successive crack patterns are shown in Figs. 6(e) and 11, respectively. In general, C1B showed good energy dissipation characteristics with the progressive increase of the drift ratio. The maximum lateral load of 18.4 kN was attained at a drift ratio of 2.0%. The specimen still stood strong with good energy dissipation throughout at a drift ratio of 3.0%. However, C1B started deteriorating at a drift ratio of 4.0% and failed to resist any additional horizontal loading after a drift ratio of 4.0% was exceeded. C1B exhibited good energy dissipation capacity, as shown in Fig. 16, as energy capacity steadily increased throughout the test. The energy dissipation was at the highest at a drift ratio of 3.0%, when the increment was near to 69% (from 4.35 to 7.38 kN m) from drift ratio of 2.0%. Limited energy was dissipated after a drift ratio 3.0% was exceeded as

shown in Fig. 16. Since there were no stirrups in its joint core, the energy dissipation capacity was mainly contributed by the beams. Fig. 11 illustrates the formation of cracking patterns of C1B. When a drift ratio of 0.67% was exceeded, cracks were found at the beam top of C1B. As illustrated in Fig. 11, it was noticeable that cracks at beams propagated rapidly when drift ratio was increased to 1.0% where several surface cracks in the joint core area were found. When a drift ratio of 1.33% was attained, cracks were found to propagate rapidly at the beam top. No new cracks were formed in the joint core area while new cracks were found at the beam bottom after a drift ratio of 1.33% was reached. Cracks at the beam bottom propagated rapidly at a drift ratio of 3.0% and joined with cracks formed at the beam top. The specimen failed at drift ratio of 3.0% when a drop in its strength was noticed. No crack was found in the column when the test was completed and no new formation of cracks at the joint core area was observed. Fig. 17(e) shows the components of the horizontal displacement measured for C1B. According to Fig. 17(e), the contribution of beam flexure, beam shear, column flexure, and joint to the total drift at 2% drift ratio were 71.6, 6.0, 3.3, and 0.0%, respectively. The contribution of beam flexure to the lateral displacement of the specimen was predominant; it varied from 51.0 to 87.3%.

Specimen C1C

Concentric Specimen C1C was an interior beam-column with a column axial load of $0.35f'_cA_g$. The measured horizontal story shear force versus horizontal displacement hysteresis loops and the successive crack patterns are shown in Figs. 6(f) and 12, respectively. The specimen in general had good energy dissipation characteristics with a large area confined within the hysteresis loops. The maximum load of 15.5 kN was attained at drift ratio of 2.0% and the specimen sustained additional horizontal load after that with good energy dissipation. The specimen began to dete-

riorate after a drift ratio of 3.0% was achieved. As shown in Fig. 16, C1C had a similar total energy absorption capacity as compared to C1B. The maximum energy dissipated of 10.2 kN m, observed at a drift ratio of 4.0%, was slightly higher than that of C1B. Similar to C1B, cracks were observed at the beam top of C1C after a drift ratio of 0.67% was exceeded. As illustrated in Fig. 12, the cracks at the beams propagated rapidly when the drift ratio was increased to 1.0%. Compared to C1B, more cracks were formed at C1C at this stage. New cracks were observed at the beam bottom after a drift ratio of 1.0% was reached. When a drift ratio of 1.33% was attained, cracks were observed to propagate rapidly at both beam top and bottom. No new cracks were formed in the joint core area while cracks at beam propagated rapidly at a drift ratio of 3.0%. The specimen failed at the drift ratio of 3.0% when a big drop in its lateral resisting capacity was observed. No cracks were observed in column and joint core after the test was completed. Fig. 17(f) shows the components of the horizontal displacement measured for C1C. The major source of the story drift was the beam displacement, indicating a "strong column weak beam" response. According to Fig. 17(f), the contribution of beam flexure, beam shear, column flexure, and joint to the total drift at 2% drift ratio were 70.5, 22.11, 0.0, and 0.0%, respectively. The contribution of beam flexure to the total drift was predominant; it varied from 51.6 to 79.2%.

Discussion of Test Results

Joint Shear Strength

Following Paulay and Priestley's (1992), suggestion the effective joint may be taken as the width of the narrower member plus a distance included between lines on a slope of 1 in 2. The γ values of all specimens were compared with FEMA 356 (2000) and NZS 3101 (Standards New Zealand 1995) as shown in Table 1. In terms of the shear strength coefficient, γ, FEMA 356 (2000)

guidelines suggest a value of 10 psi or 0.83 MPa for an interior joint without transverse beams and ρ" less than 0.003. The tests conducted at NTU showed that FEMA 356 (2000) guidelines were unconservative for predicting the joint shear performance of the specimens with a column to beam width ratio of about 3.56. The γ values of eccentric and concentric specimens were, respectively, only around 75 and 60% of the value suggested by FEMA 356 (2000). According to NZS 3101 (Standards New Zealand 1995), for interior beam-column joints with nonseismically detailing, the maximum joint shear stress is between $0.11f'_c$ and $0.17f'_c$. This correlates well with the experimental results of the specimens with column to beam width ratio of about 3.56, consistent with similar test conducted by Li et al. (2002) at NTU, when the specimens, with a beam to column width ratio of about 3, were tested with a zero column axial load. Based on the limited test data, using the lower value of the NZS range (Standards New Zealand 1995), $0.11f'_c$, gives the lower bound for the maximum shear stress of the nonseismically detailed joints that has a column to beam width ratio from 0 to 3.56. The effects of column axial load level were not significant in comparison with E1A, E1B, and E1C or C1A, C1B, and C1C as the γ value achieved was similar in all specimens. It is known that the column flexural strength to beam flexural strength ratios significantly affects the global as well as the local behavior of the specimens. As shown in Table 1, the column flexural strength to beam flexural strength ratios of E1A (C1A), E1B (C1B), and E1C (C1C) were 4.62, 5.23, and 6.36, respectively. These satisfied the strong column-weak beam criterion. The failure of the beam in a weak beam-strong column combination could have overridden the effect of column axial loading. The observation of excessive cracking along the beams during the tests supports this hypothesis.

As illustrated in Fig. 7, the cracks in the joint area of Specimen E1A were extended from the

flushed surface to the offset surface. However, the cracks in the joint area of Specimens E1B and E1C were observed only on the flushed surface. It showed strong evidence that the effective joint width varied under different axial compression loading. Moreover, the failure behavior of the specimens was controlled by the failure of the beam in a weak beam-strong column combination; it is unreliable to use the above joint shear strength values to justify the effects of axial compression loading to the joint behavior.

Effect of Axial Compression Loading

Beneficial Effects of Bond Strength Caused by Axial Compression Loading

It has long been known that clamping pressure exerted on the anchored bars enhances the bond strength. This beneficial effect of column axial loads was recognized in NZS 3101 (Standards New Zealand 1995). NZS 3101 (Standards New Zealand 1995) recommends the coefficient α_p to allow for the beneficial effect of compression in a column

$$\alpha_p = \frac{P}{2f'_c A_g} + 0.95 \quad (1)$$

If the bond strength u_a is equal to $1.2\sqrt{f'_c}$ when axial compression loading is zero, the bond strength under different column axial loads is calculated as

$$u_a = 1.2\sqrt{f'_c}\left(\frac{P}{2f'_c A_g} + 0.95\right) \quad (2)$$

Fig. 18 shows the maximum bond stress of all specimens. It is noted that the trend found here is close to that given by NZS 3101 (Standards New Zealand 1995).

Beneficial Effects of Axial Compression Loading on Joint Shear Resistance

Specimens E1A and E1B obtained the maximum diagonal compressive strain of 0.007 and

0.0038, respectively. However, the maximum diagonal compressive strain of Specimen E1C during the test was 0.0003, which was much smaller than the strain in the concrete cylinder at peak stress. It showed that column axial loading helped to reduce the applied shear force in the diagonal compressive strut. The enhancement of bond strength could have led to the reduction of the applied shear force to the diagonal strut. In addition, column axial loading also helped to increase the size of the diagonal compressive strut, helping to enhance the capacity of the diagonal compressive strut.

Effects of Axial Compression Loading on Torsional Deformations

Specimens E1A, E1B, and E1B obtained the maximum torsional rotation of 0.0061, 0.0053, and 0.0040, respectively, as shown in Fig. 19. It showed that column axial loading helped to reduce the torsional rotations in tested interior beam-column joints.

Detrimental Effects of Axial Compression Loading on Bond Deterioration

The degradation of anchorage resistance in beam bars passing the joint was observed in all specimens. Thus, the compressive stress in the compression reinforcement bars decreased and changed to tension as illustrated in Fig. 13. Bond deterioration occurred along the beam bars of all specimens. Since bond condition is determined mainly by the ratio of the beam and column bar diameter to the column and beam depths, and the ratio of beam bar diameter to the column depth of all specimens of 1/22 does not satisfy the requirement given by NZS 3101 (Standards New Zealand 1995), it is not surprising that bond deterioration occurred along the beam bars.

The beneficial effects of axial compression loading on the average bond strength were recognized. It explains the attainment of higher stiffness and energy dissipation capacity of E1C (C1C) than E1A (C1A) and E1B (C1B) at the first few drift ratios as shown in Figs. 15 and 16.

However, when the bond resistance reached its maximum value and started to degrade, the presence of axial compression loading tended to accelerate the bond deterioration. As illustrated in Fig. 13, at a drift ratio of 2.0%, the compression reinforcements of Specimens E1C and C1C attain tensile yielding, indicating anchorage failure. However at this drift ratio, a sufficient amount of bond resistance still exists in Specimens E1A, E1B, C1A, and C1B, which is attributed to lower attainment of energy dissipation capacity and stiffness of E1C (C1C) than E1A (C1A) and E1B (C1B) at this stage as shown in Figs. 15 and 16. It could be concluded that before the bond resistance reached its maximum value, the presence of axial compression loading helped to enhance stiffness and energy dissipation capacity. However, when the bond resistance reached its maximum value and started to degrade, the presence of axial compression loading accelerates the stiffness degradation and reduces the energy dissipation capacity.

Effect of Eccentricity on Behavior of Joints

Confinement Effects on Joint Shear Resistance

The diagonal compressive strains of diagonal strut of Specimens C1A, C1B, and C1C were extremely small throughout the tests. This indicates that either the strut mechanism of C1A, C1B, and C1C was still strong up to a drift ratio of 4.0% or the diagonal strut of these specimens was still able to sustain additional loading at this stage. However, Specimens E1A and E1B obtained the maximum diagonal compressive strains of 0.007 and 0.0038 at failure, respectively. This is attributed to the beneficial effects of confinement on concentric joints.

Effects of Eccentricity on Global Behavior

Specimens E1A and E1B obtained higher energy dissipation capacity and lower stiffness than C1A and C1B throughout the tests as illustrated in Figs. 15 and 16. It is attributed to the effect of

eccentricity. However, Specimen E1C and C1C showed similar energy dissipation capacity and stiffness degradation trends. At a drift ratio of 4.0%, the energy dissipation capacities of E1C and C1C were 10.3 and 10.2 kN m, respectively. The beam failure in the specimens with high axial compression loading, E1C, and C1C, could have overridden the effect of eccentricity. This explains similar energy dissipation and stiffness degradation obtained by E1C and C1C.

Conclusions

The present investigation is concerned with the assessment of reinforced concrete interior beam-wide column joints, which are often found in the framed structures with nonseismic detailing in Singapore. The research has shown that the joints attained interstate drifts of 2.0% without significant degradation. The attainment of low stiffness and strength was attributed to the bond deterioration of the longitudinal bars through the joint core. In all test specimens, the ratios of column moments over beam moments are very high. It could be concluded that the energy dissipation of the joints is mainly focused on the beams. The failure of beams in strong column-weak beam joints could have overridden the effects of column axial loading in the test specimens in terms of global behaviors.

This beneficial effect of column axial loading on bond strength was observed in the test specimens. The bond strengths found in the experiments are close to that given by NZS 3101 (Standards New Zealand 1995). In addition, experimental results showed that before the bond resistance reached its maximum value, the presence of axial compression loading is beneficial to energy dissipation capacity and stiffness of joints. However, after the bond resistance reached its maximum value and started to degrade, the presence of axial compression loading has detrimental effects on energy dissipation capacity and stiffness of joints.

At axial compression loading level of less than $0.1f'_cA_g$, eccentric specimens obtained higher energy dissipation capacity and lower stiffness than concentric ones as expected. However at axial compression loading of $0.35f'_cA_g$, similar energy dissipation capacity and stiffness degradation was observed in both concentric and eccentric specimens. The anchorage failure of these specimens could have overridden the effect of eccentricity.

The maximum nominal horizontal shear stresses of the test specimens correlate well with NZS 3101 (Standards New Zealand 1995), which suggested the maximum joint shear stress for interior beam-column joints with nonseismically detailing to be between $0.11f'_c$ and $0.17f'_c$. This is consistent with the conclusions drawn by Li et al. (2002). Based on the limited test data, the lower value of the NZS 3101 range (Standards New Zealand 1995), $0.11f'_c$ can be used to give the maximum shear stress lower bound of the test results.

Acknowledgments

The financial assistance provided by the Building & Construction Authority and Ove Arup, Singapore, is gratefully acknowledged.

Notation

The following symbols are used in this paper:

A_g = gross sectional area of column;

bj = effective joint width;

b_w = width of beam;

DR = story drift ratio;

f'_c = concrete compressive strength;

f_y = yield strength of reinforcement;

h_c = column depth;

P = axial compressive column load;

u_a = maximum bond stress;

V_{jh} = joint shear force;

v_{jh} = nominal joint shear stress; and

γ = joint shear strength coefficient.

References

American Concrete Institute (ACI) Committee 318. (2002). *Building code requirements for structural concrete (ACI 318–02) and commentary (ACI 318R-02)*, Farmington Hills, Mich.

Architectural Institute of Japan (AIJ). (1994). *Design guidelines for earthquake resistant reinforced concrete buildings based on ultimate strength concept (drift) and commentary*, Tokyo.

British Standards Institute (BSI). (1997). *Structural use of concrete, Part 1. Code of practice for design and construction, BS 8110*, London.

Federal Emergency Management Agency (FEMA). (2000). "Prestandard and commentary for the seismic rehabilitation of buildings." *FEMA 356*, Washington, D.C.

Joh, O., Goto, Y., and Shibata, T. (1991). *Behavior of reinforced concrete beam-column joints with eccentricity, SP-123*, J. O. Jirsa, ed., American Concrete Institute, Farmington Hills, Mich., 317–357.

Joint ACI-ASCE Committee 352. (1985). "Recommendations for design of beam-column joints in monolithic reinforced concrete structures." *J. Am. Concr. Inst.*, 82(3), 266–283.

Lawrance, G. M, Beattie, G. J., and Jacks, D. H. (1991). "The cyclic load performance of an eccentric beam-column Joint." *Rep. No. 91-25126*, Central Laboratories, Lower Hutt, New Zealand.

Li, B., Wu, Y. M., and Pan, T. C. (2002). "Seismic behaviour of nonseismically detailed interior beam-wide column joints—Part I: experimental results and observed behavior." *ACI Struct. J.*, 99(6), 791– 802.

Paulay, T., and Priestley, M. J. N. (1992). *Seismic design of reinforced concrete masonry buildings*, Wiley, New York.

Raffaelle, G. S., and Wight, J. K. (1995). “Reinforced concrete eccentric beam-column connections subjected to earthquake-type loading.” *ACI Struct. J.*, 92(1), 45–55.

Shin, M., and LaFave, J. M. (2004). “Seismic performance of reinforced concrete eccentric beam-column connections with floor slabs.” *ACI Struct. J.*, 101(3), 403–412.

Standards New Zealand (1995). “Concrete structures standard (1995). Part 1: The design of concrete structure.” *NZS 3101*, New Zealand.

Teng, S., and Zhou, H. (2003). “Eccentric reinforced concrete beam-column joints subjected cyclic loading.” *ACI Struct. J.*, 100(2), 139– 148.

List of Tables

List of Figures

Specimen	$P/A_g f'_c$	v_{jh} (MPa)	γ	v_{jh}/f'_c	NZS-3101	FEMA-356	$(EI)_C/(EI)_B$	$\Sigma M_C/\Sigma M_B$	$\gamma/\gamma_{Fema356}$ (%)
C1A	0.00	2.08	$0.47\sqrt{f'_c}$	$0.11f'_c$	$0.11f'_c - 0.17f'_c$	$0.83\sqrt{f'_c}$	2.9	4.62	56.6
C1B	0.10	2.16	$0.48\sqrt{f'_c}$	$0.11f'_c$	$0.11f'_c - 0.17f'_c$	$0.83\sqrt{f'_c}$	2.9	5.23	57.8
C1C	0.35	2.21	$0.49\sqrt{f'_c}$	$0.11f'_c$	$0.11f'_c - 0.17f'_c$	$0.83\sqrt{f'_c}$	2.9	6.36	59.0
E1A	0.00	2.55	$0.57\sqrt{f'_c}$	$0.13f'_c$	$0.11f'_c - 0.17f'_c$	$0.83\sqrt{f'_c}$	2.9	4.62	73.5
E1B	0.10	2.67	$0.60\sqrt{f'_c}$	$0.13f'_c$	$0.11f'_c - 0.17f'_c$	$0.83\sqrt{f'_c}$	2.9	5.23	73.5
E1C	0.35	2.72	$0.61\sqrt{f'_c}$	$0.14f'_c$	$0.11f'_c - 0.17f'_c$	$0.83\sqrt{f'_c}$	2.9	6.36	74.7

Table 1

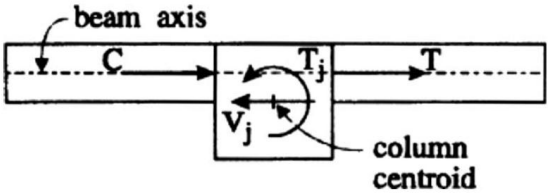

Fig. 1

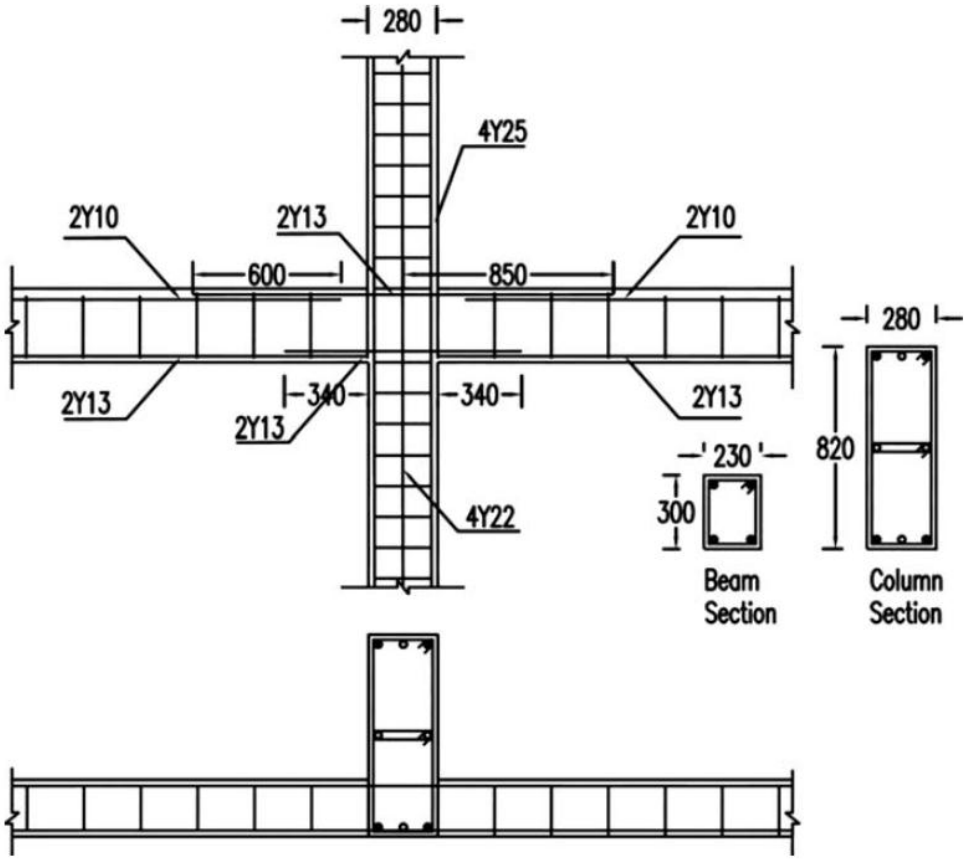
280
4Y25
2Y10
2Y13
2Y10
600
850
2Y13
340
340
2Y13
2Y13
4Y22
230
300
Beam
Section
280
820
Column
Section

Fig. 2

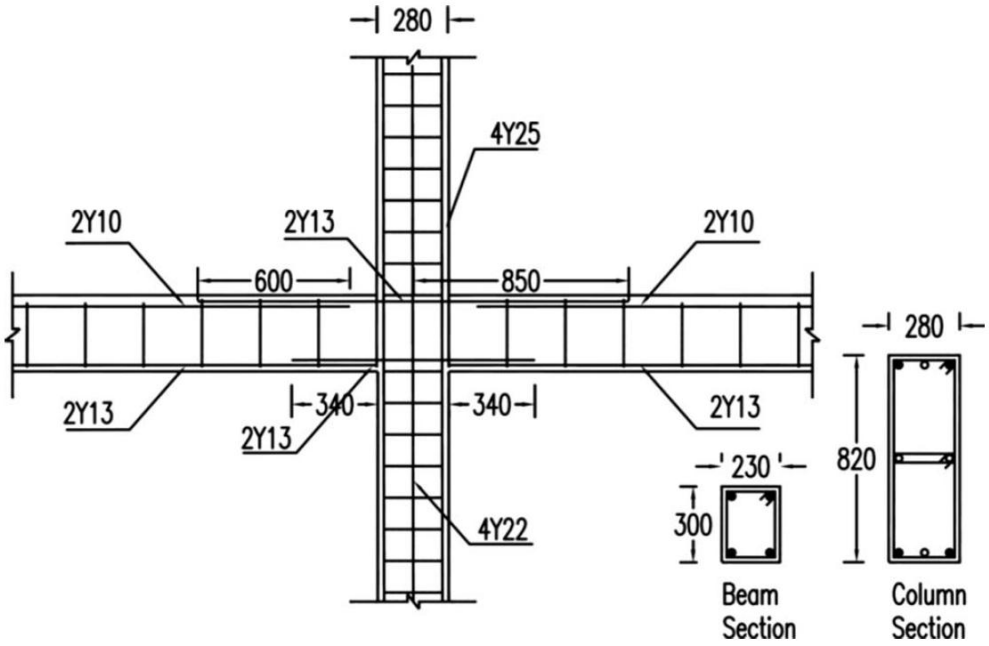
280
4Y25
2Y10
2Y13
2Y10
600
850
280
2Y13
340
340
2Y13
2Y13
230
820
300
4Y22
Beam
Section
Column
Section

Fig. 3

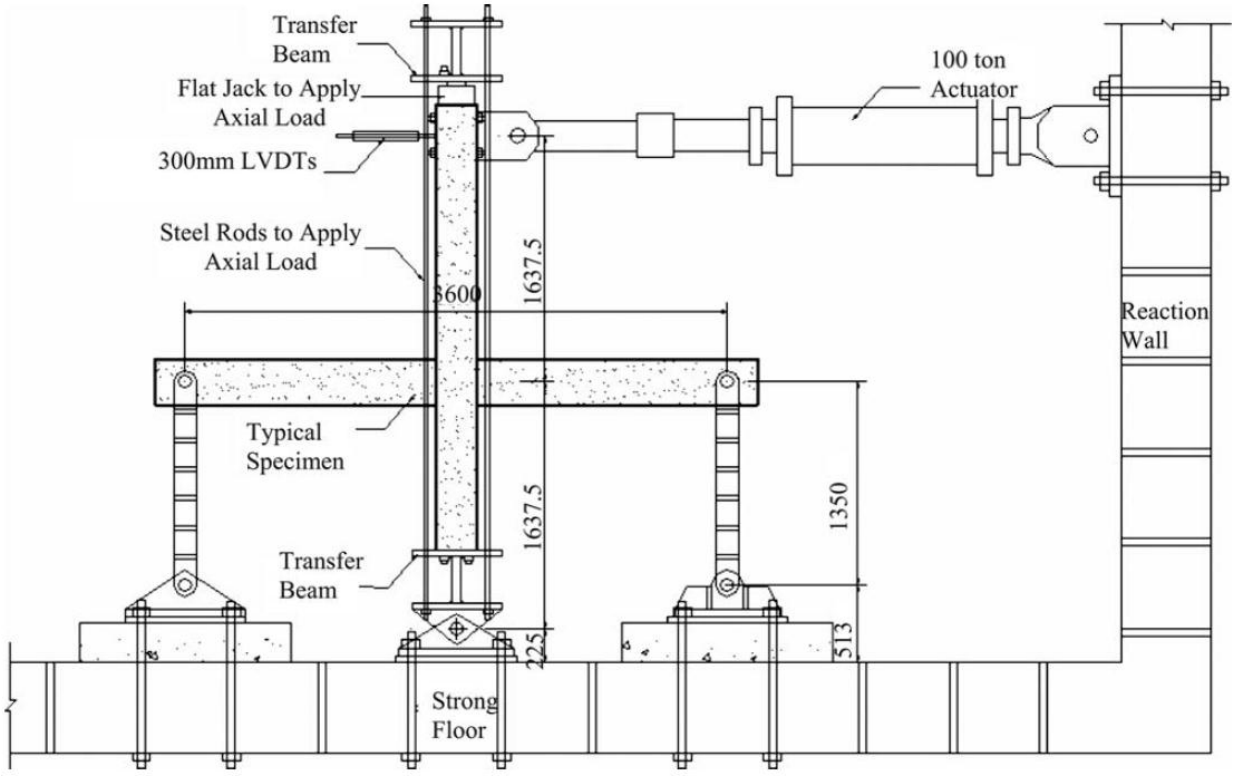
Transfer
Beam
Flat Jack to Apply
Axial Load
300mm LVDTs
Steel Rods to Apply
Axial Load
3600
1637.5
100 ton
Actuator
Reaction
Wall
Typical
Specimen
1637.5
1350
Transfer
Beam
225
513
Strong
Floor

Fig. 4

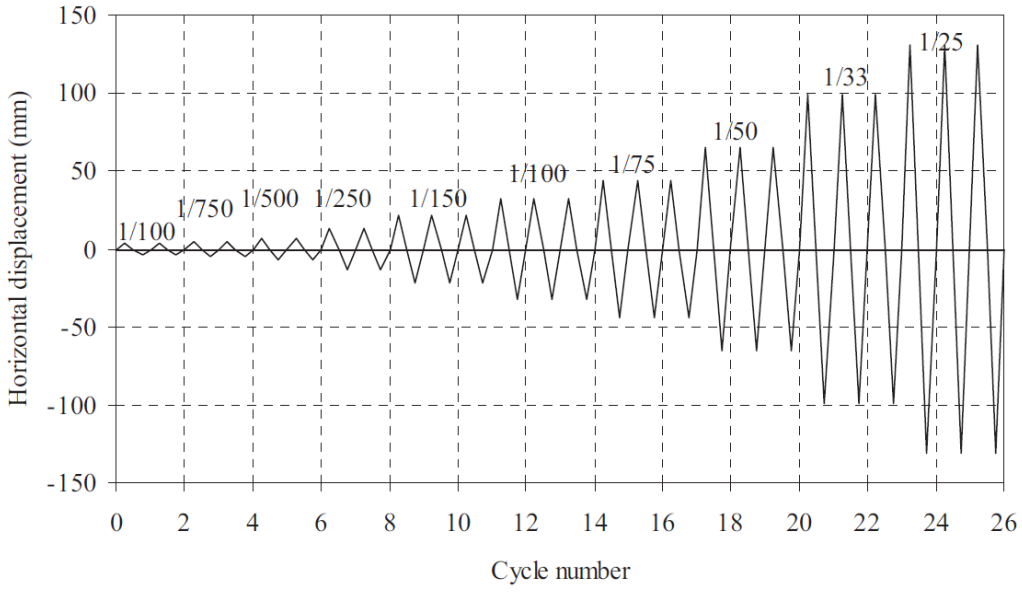
Horizontal displacement (mm)
150
100
50
0
-50
-100
-150
0
2
4
6
8
10
12
14
16
18
20
22
24
26
Cycle number
1/100
1/750
1/500
1/250
1/150
1/100
1/75
1/50
1/33
1/25

Fig. 5

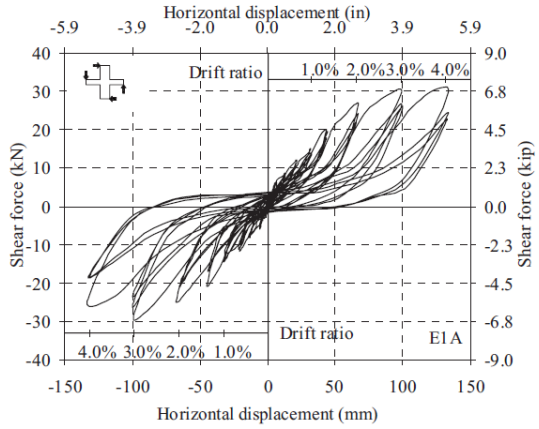
Horizontal displacement (in)
Drift ratio
1.0% 2.0% 3.0% 4.0%
Drift ratio
4.0% 3.0% 2.0% 1.0%
E1A
Shear force (kN)
Shear force (kip)
Horizontal displacement (mm)

(a)

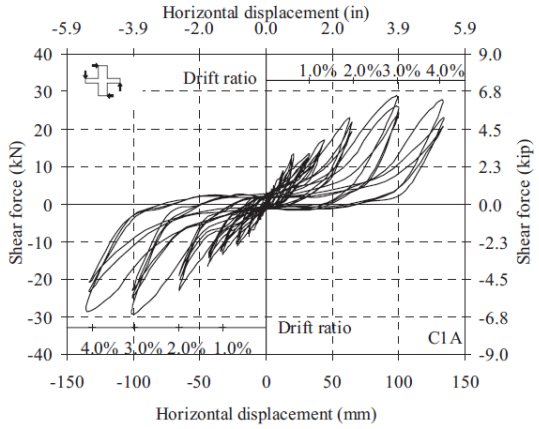
Horizontal displacement (in)
Drift ratio
1.0% 2.0% 3.0% 4.0%
Drift ratio
4.0% 3.0% 2.0% 1.0%
C1A
Shear force (kN)
Shear force (kip)
Horizontal displacement (mm)

(d)

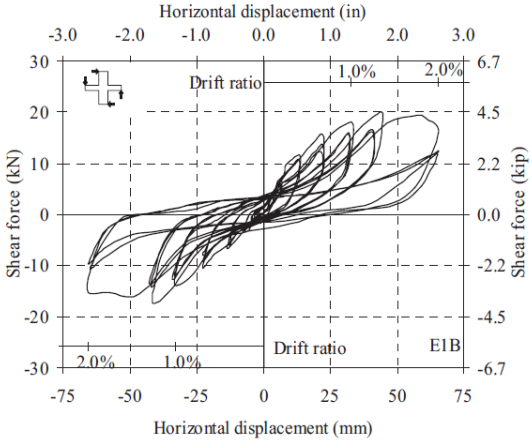
Horizontal displacement (in)
Drift ratio
1.0%
2.0%
Drift ratio
2.0%
1.0%
E1B
Shear force (kN)
Shear force (kip)
Horizontal displacement (mm)

(b)

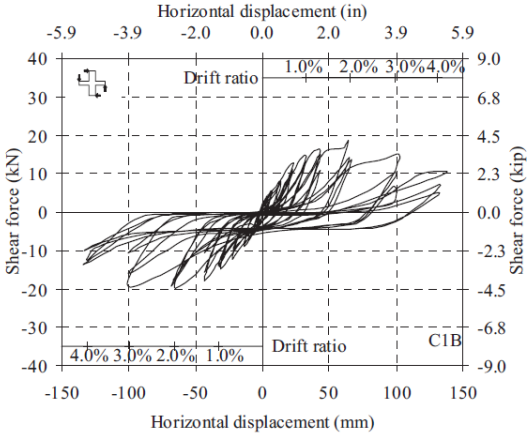
Horizontal displacement (in)
Drift ratio
1.0% 2.0% 3.0% 4.0%
Drift ratio
4.0% 3.0% 2.0% 1.0%
C1B
Shear force (kN)
Shear force (kip)
Horizontal displacement (mm)

(e)

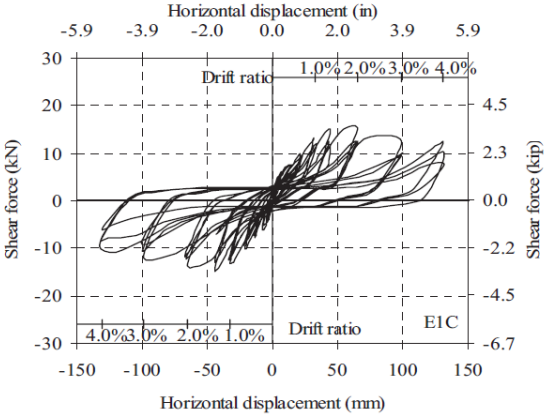
Horizontal displacement (in)
Drift ratio
1.0% 2.0% 3.0% 4.0%
Drift ratio
4.0% 3.0% 2.0% 1.0%
E1C
Shear force (kN)
Shear force (kip)
Horizontal displacement (mm)

(c)

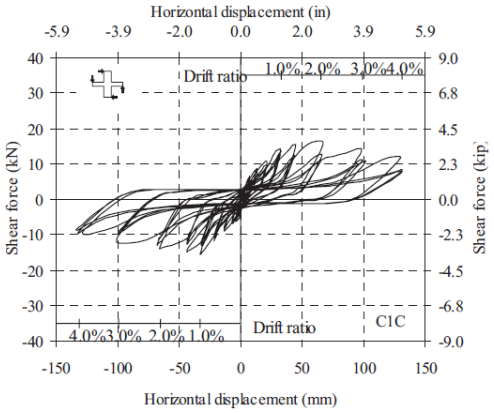
Horizontal displacement (in)
Drift ratio
1.0% 2.0% 3.0% 4.0%
Drift ratio
4.0% 3.0% 2.0% 1.0%
C1C
Shear force (kN)
Shear force (kip)
Horizontal displacement (mm)

(f)

Fig. 6

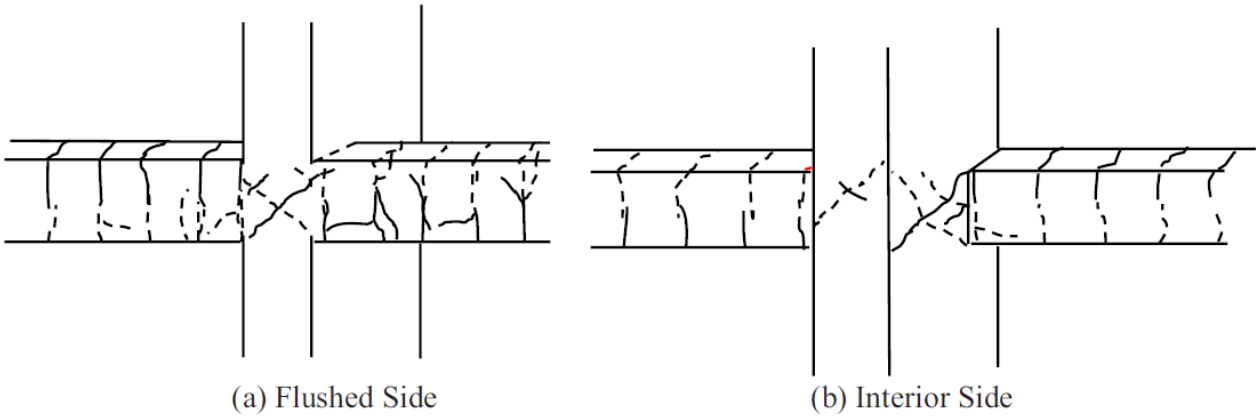

(a) Flushed Side (b) Interior Side

Fig. 7

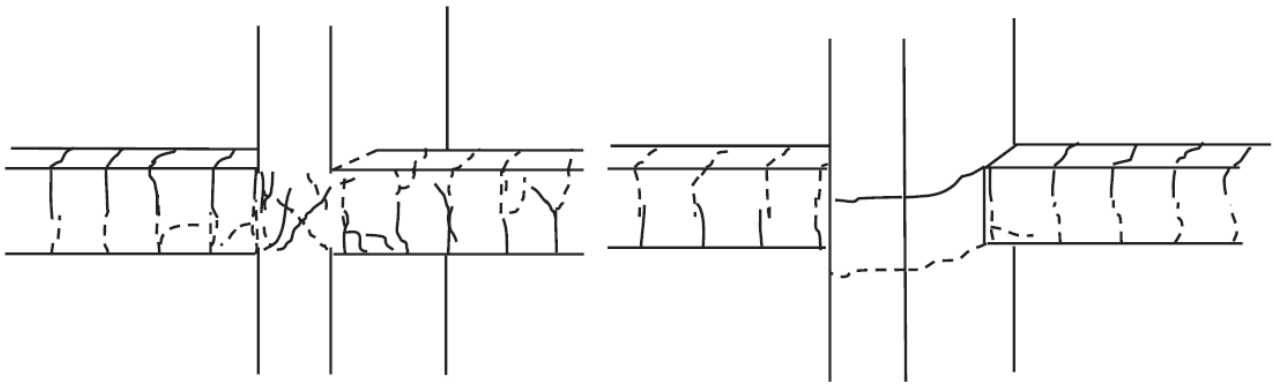

(a) Flushed Side (b) Interior Side

Fig. 8

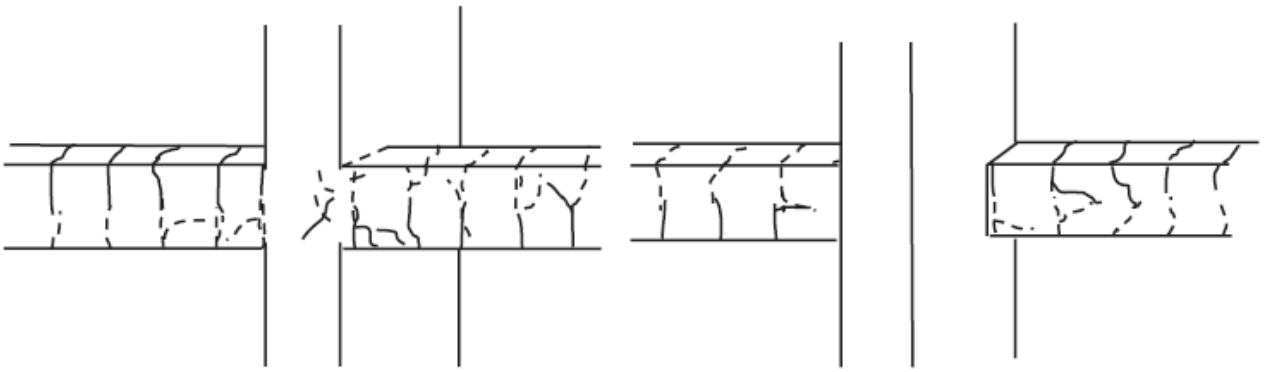

(a) Flushed Side (b) Interior Side

Fig. 9

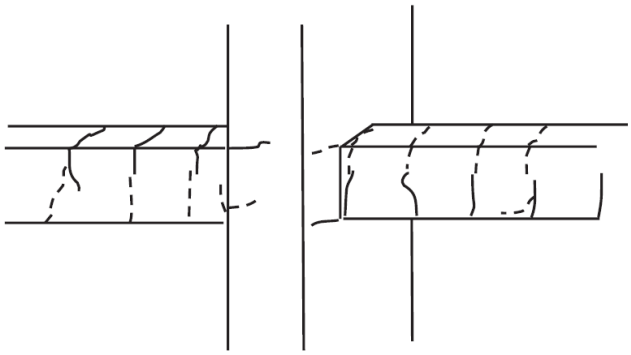

Fig. 10

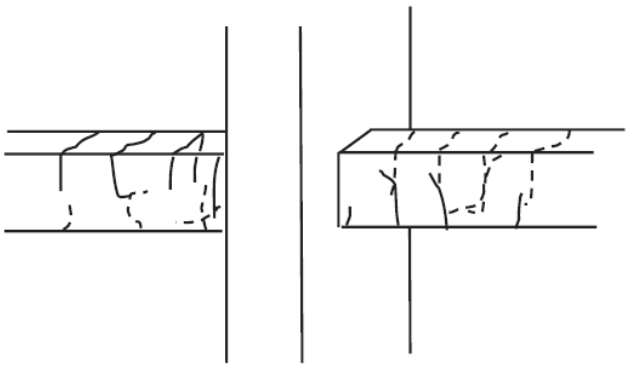

Fig. 11

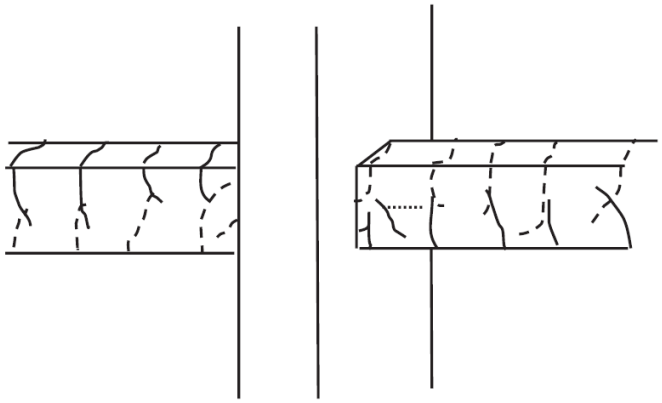

Fig.12

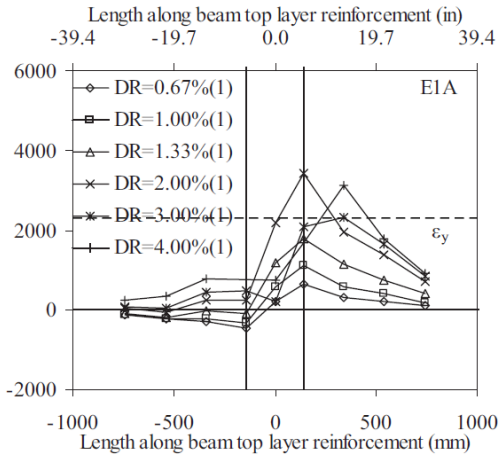

(a)

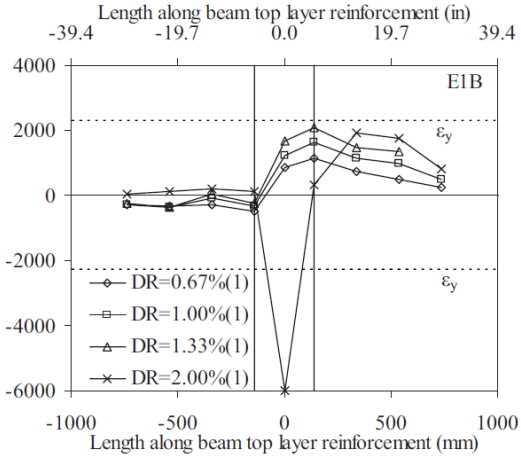

(b)

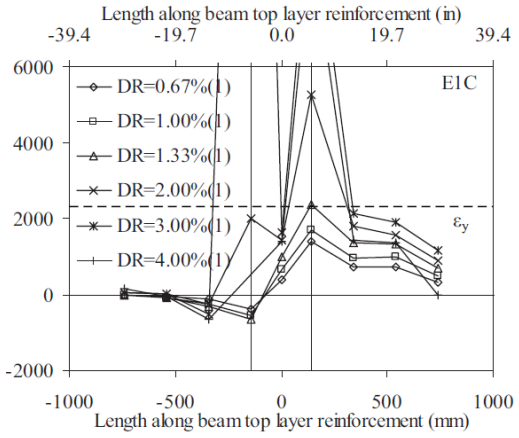

(c)

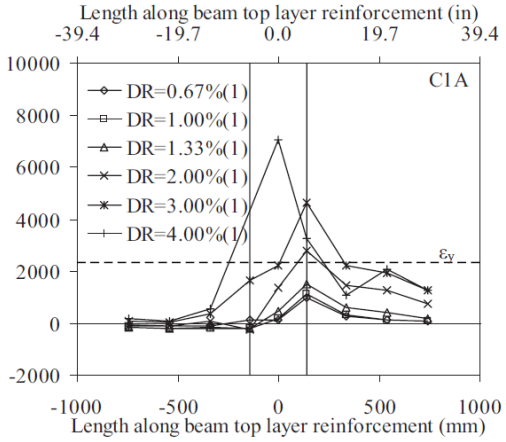

(d)

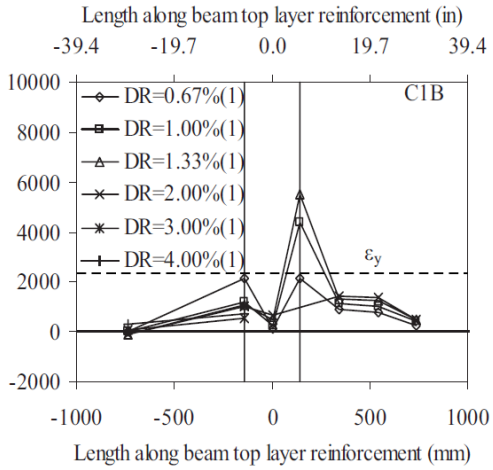

(e)

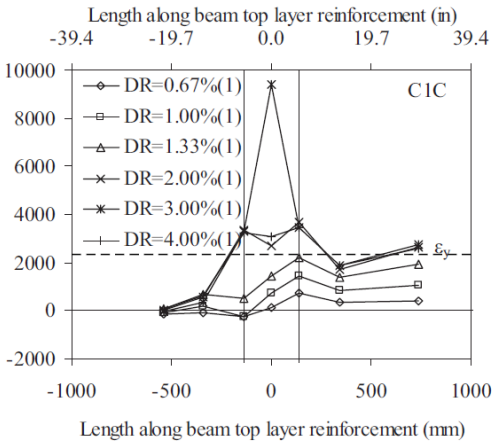

(f)

Fig. 13

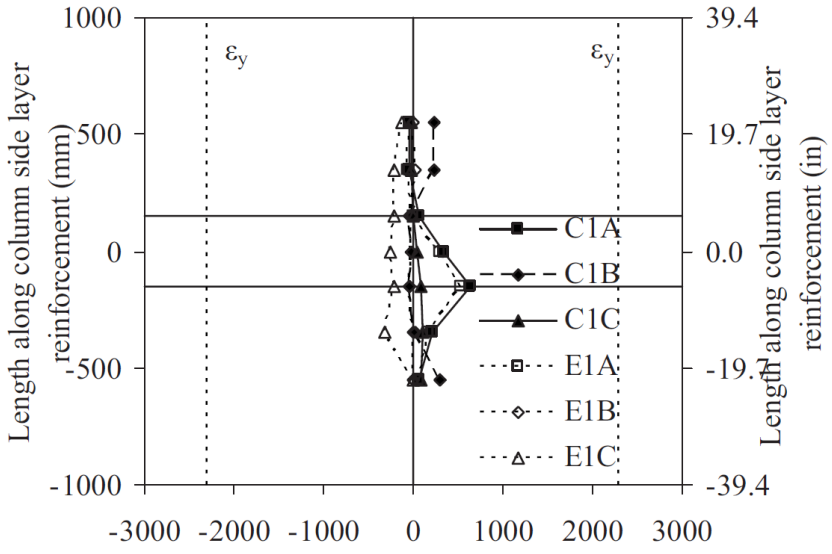
1000
500
0
-500
-1000
39.4
19.7
0.0
-19.7
-39.4
-3000
-2000
-1000
0
1000
2000
3000
εy
εy
Length along column side layer reinforcement (mm)
Length along column side layer reinforcement (in)
C1A
C1B
C1C
E1A
E1B
E1C

Fig. 14

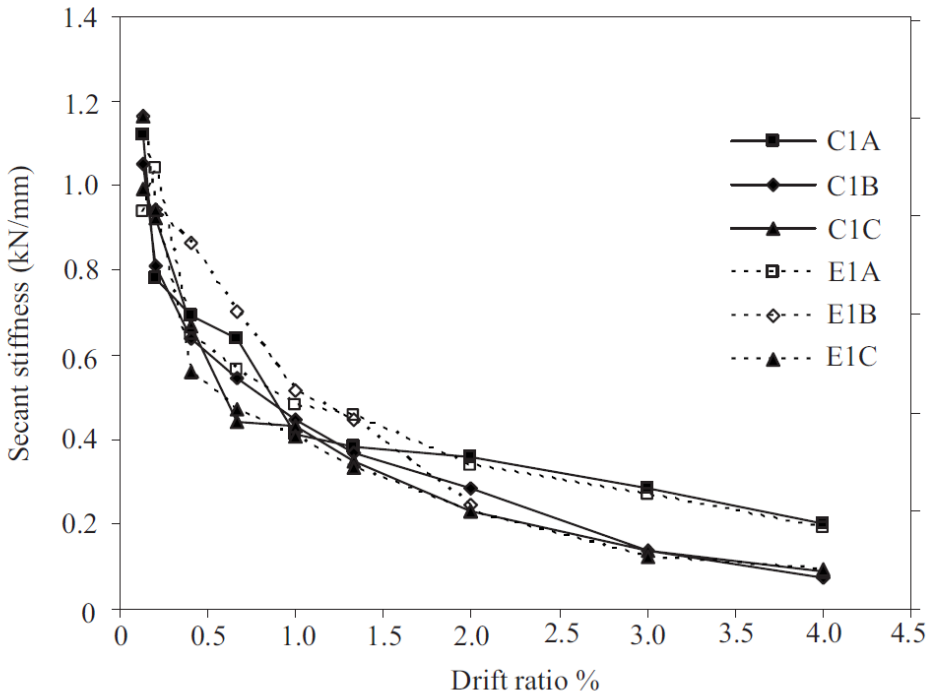
1.4
1.2
1.0
0.8
0.6
0.4
0.2
0
Secant stiffness (kN/mm)
0
0.5
1.0
1.5
2.0
2.5
3.0
3.5
4.0
4.5
Drift ratio %
C1A
C1B
C1C
E1A
E1B
E1C

Fig. 15

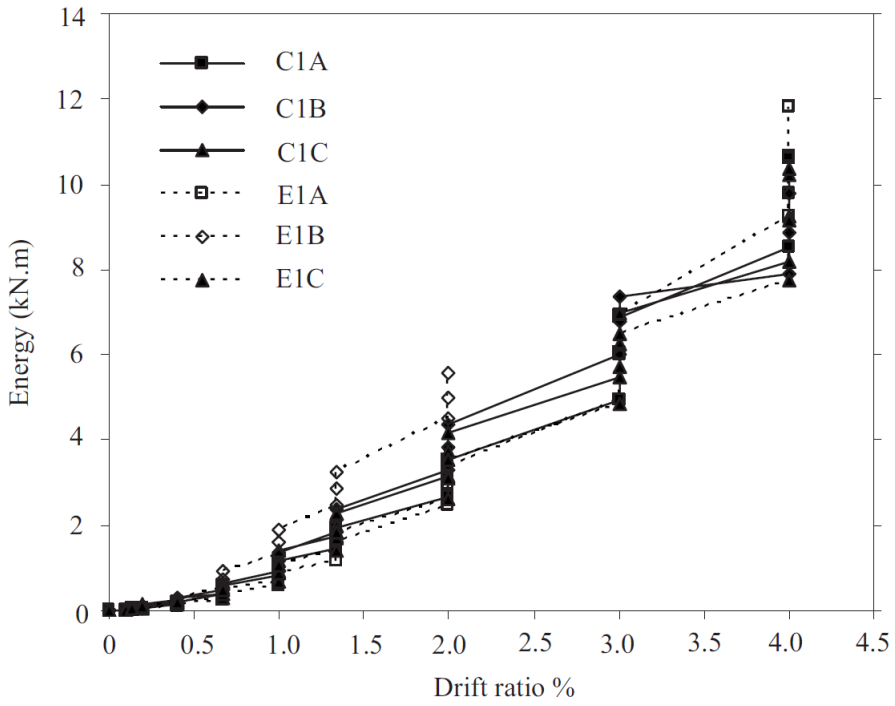
14
12
10
8
6
4
2
0
Energy (kN.m)
C1A
C1B
C1C
E1A
E1B
E1C
0
0.5
1.0
1.5
2.0
2.5
3.0
3.5
4.0
4.5
Drift ratio %

Fig. 16

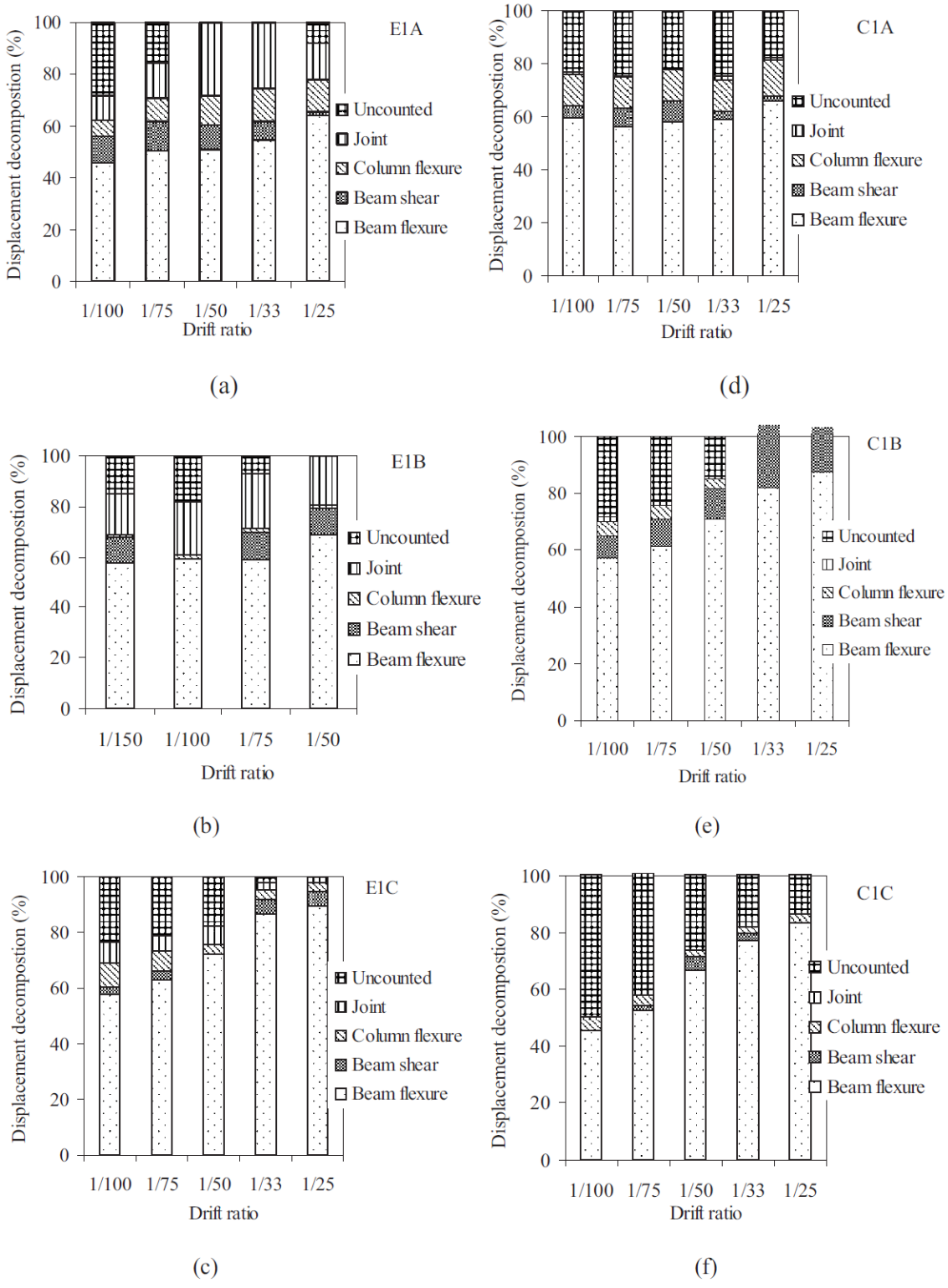
E1A
Displacement decompostion (%)
100
80
60
40
20
0
Uncounted
Joint
Column flexure
Beam shear
Beam flexure
1/100 1/75 1/50 1/33 1/25
Drift ratio
(a)
C1A
Displacement decompostion (%)
Uncounted
Joint
Column flexure
Beam shear
Beam flexure
1/100 1/75 1/50 1/33 1/25
Drift ratio
(d)
E1B
Displacement decompostion (%)
Uncounted
Joint
Column flexure
Beam shear
Beam flexure
1/150 1/100 1/75 1/50
Drift ratio
(b)
C1B
Displacement decompostion (%)
Uncounted
Joint
Column flexure
Beam shear
Beam flexure
1/100 1/75 1/50 1/33 1/25
Drift ratio
(e)
E1C
Displacement decompostion (%)
Uncounted
Joint
Column flexure
Beam shear
Beam flexure
1/100 1/75 1/50 1/33 1/25
Drift ratio
(c)
C1C
Displacement decompostion (%)
Uncounted
Joint
Column flexure
Beam shear
Beam flexure
1/100 1/75 1/50 1/33 1/25
Drift ratio
(f)

Fig. 17

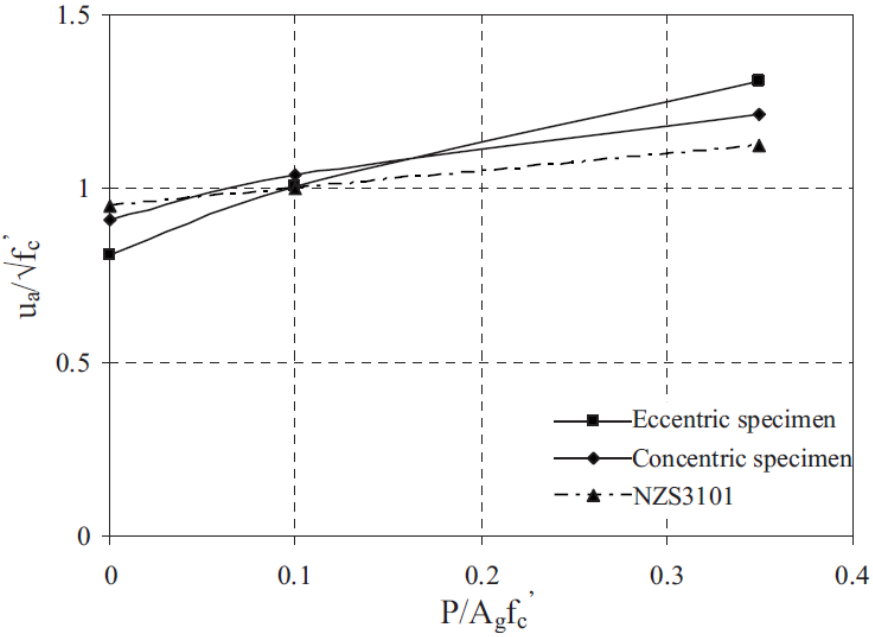
1.5
1
0.5
0
0
0.1
0.2
0.3
0.4
$u_a/\sqrt{f_c'}$
$P/A_g f_c'$
Eccentric specimen
Concentric specimen
NZS3101

Fig. 18

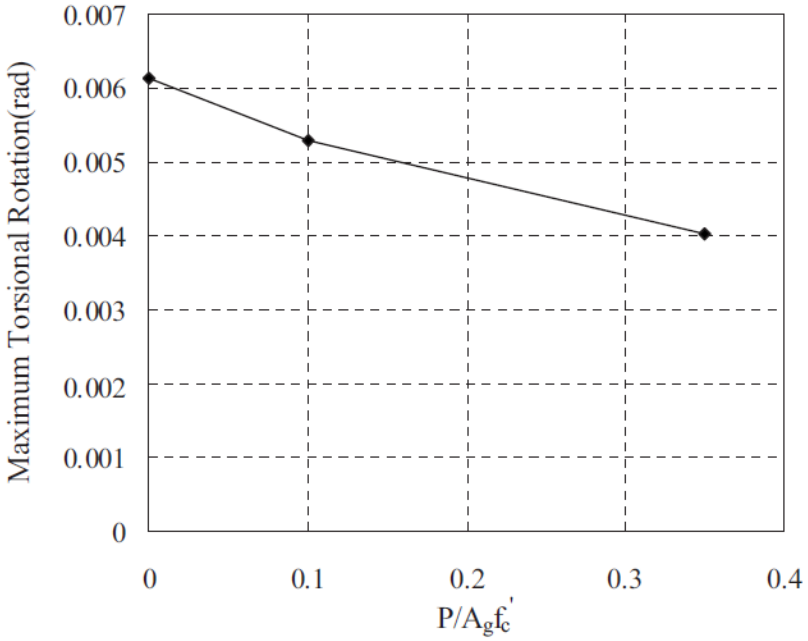
0.007
0.006
0.005
0.004
0.003
0.002
0.001
0
Maximum Torsional Rotation(rad)
0
0.1
0.2
0.3
0.4
P/A_g f_c'

Fig. 19